

Inelastic pion scattering for $1p$ -shell targets

T.-S. H. Lee and D. Kurath

Argonne National Laboratory, Argonne, Illinois 60439

(Received 2 August 1979)

Inelastic scattering of pions with energy near the (3,3) resonance is calculated with a distorted-wave impulse approximation formulated in momentum space. Results for all $1p$ -shell targets are given and compared to existing data. Strong transitions are dominated by quadrupole amplitudes, and enhancement factors consistent with observed $B(E2)$ values are needed to attain agreement with observed cross sections in these cases. The sensitivity of pion scattering to isospin effects is noted. This distorted-wave impulse approximation approach appears to offer a reasonable interpretation of inelastic pion scattering.

NUCLEAR REACTIONS, NUCLEAR STRUCTURE (π, π') $E_{\pi} \approx 120$ to 220 MeV; $1p$ -shell targets, theoretical $d\sigma/d\Omega$ based on DWIA in momentum space; effect of nuclear structure and sensitivity to isospin.

I. INTRODUCTION

In this paper we study the inelastic scattering of intermediate energy pions from $1p$ -shell nuclei within the framework of the distorted-wave impulse approximation (DWIA). The method of Lee and Tabakin¹ is extended to obtain a general formulation of DWIA in momentum space, and the objective is to examine to what extent this method is valid in the region of energy near the (3,3) resonance by treating excitation of $1p$ -shell nuclei for which reasonably well-tested wave functions are available from the calculation of Cohen and Kurath.²

In the DWIA procedure it is assumed that the pion-nucleus interaction potentials are determined using only the initial and final nuclear wave functions and the πN off-shell t matrix. Higher order effects such as caused by true pion-absorption and by channel-coupling are neglected. In contrast to other DWIA calculations based on the Kisslinger or Laplacian models,³ the main feature of our approach is to construct the πN off-shell t matrix with the finite range πN model of Londergan, McVoy, and Moniz.⁴ The t matrix is generated directly by the available momentum-space elastic

scattering program, PIPIT.⁵ In view of the general success in describing elastic scattering at resonance energies with PIPIT, this approach should suffice for our purpose.

As our primary emphasis is to investigate the validity of the DWIA, we first study inelastic scattering in cases where the $1p$ -shell model adequately describes some other experimentally observed process such as gamma decay or inelastic electron scattering. Since the comparison with experiment for these cases is reasonably encouraging, we then treat other cases wherein various features of the πN interaction are emphasized and where a comparison with experiment will show the extent to which this DWIA method is a valuable tool.

In Sec. II we present the momentum-space formalism of the DWIA in the shell-model representation, briefly reviewing the numerical method of Ref. 1. Section III contains the form and numerical values of the one-body transition density matrix elements obtained from the shell-model calculation of Ref. 2. In Sec. IV calculated cross sections are presented for inelastic π^{\pm} scattering and for the (π^+, π^0) reaction. Comparison with experiment is included for available data. Section V is devoted to discussion and summary.

II. MOMENTUM-SPACE FORMULATION OF DWIA

In the momentum-space representation, the DWIA amplitude for inelastic scattering is

$$T_{fi}(\vec{k}'_0 \Lambda', \vec{k}_0 \Lambda) = \int d\vec{k}' \int d\vec{k} \chi_{k_0 \Lambda'}^{(+)*}(\vec{k}') U_{fi}(\vec{k}' \Lambda', \vec{k} \Lambda, E) \chi_{k_0 \Lambda}^{(+)}(\vec{k}). \quad (1)$$

Here the \vec{k} 's are relative momenta of pion and nucleus in the π -nucleus center-of-mass frame. The isospin z components of the pions are denoted by Λ and the nuclear state label denotes angular momentum and isospin quantum numbers, $|i\rangle = |(JMT\Lambda)_i\rangle$. The distorted waves are calculated from the optical potential $U_{\alpha\alpha}(E)$ by solving the relativistic scattering equation

$$|\chi_{\vec{k}_0 a}^{(\pm)}\rangle = |\vec{k}_0\rangle + \left(\frac{1}{E - E_\pi(\vec{k}) - E_A(\vec{k}_J \pm i\epsilon)} \right) U_{aa}(E) |\chi_{\vec{k}_0 a}^{(\pm)}\rangle. \quad (2)$$

The pion-nucleus interaction potential $U_{fi}(E)$ is evaluated starting from the impulse approximation

$$U_{fi}(\vec{k}' \Lambda', \vec{k} \Lambda) = \left\langle f \left| \sum_{n=1}^A t_n(\vec{k}', \vec{k}, W_0) e^{i(\vec{k}' - \vec{k}) \cdot \vec{r}_n} \right| i \right\rangle. \quad (3)$$

Note that the πN off-shell t matrix, t_n in Eq. (3), is an operator in spin-isospin space. Following Ref. 1 we make a multipole expansion

$$t(\vec{k}', \vec{k}, W_0) = \sum_{\lambda m S I} t_S^{\lambda I}(k', k, W_0) Y_{\lambda m}^*(\hat{k}') [Y_\lambda(\hat{k}) \times \sigma_S]_{\lambda m P_I}, \quad (4)$$

where $\sigma_1 = \vec{\sigma}$, $\sigma_0 = 1$, and $[Y_\lambda \times \sigma_S]$ indicates vector coupling. Here P_I is the operator which projects onto the πN isospin states $I = \frac{3}{2}$ or $I = \frac{1}{2}$. The spin-dependent ($S=1$) and spin-independent ($S=0$) πN forces are given by

$$t_S^{\lambda I}(k', k, W_0) = 4\pi [(-1)^{\lambda-1} / (2\lambda)^{1/2}] \sum_J \hat{J} \begin{pmatrix} \lambda & \frac{1}{2} & J \\ -S & S - \frac{1}{2} & \frac{1}{2} \end{pmatrix} f_{\lambda J}^I(k', k, W_0), \quad (5)$$

where we introduce the abbreviation $\hat{J} \equiv 2J+1$, and the bracket inside the summation is a $3J$ symbol. The quantities $f_{\lambda J}^I$ are computed directly from the πN model of Ref. 4 by means of the program⁵ PIPIT.

By substituting Eq. (4) into Eq. (3) we obtain a partial wave decomposition of the interaction potential U_{fi} which generalizes the results of Ref. 1,

$$U_{fi}(\vec{k}' \Lambda', \vec{k} \Lambda) = \sum_{LML'M'\mathcal{G}\mathcal{T}} [\hat{L}\hat{L}'\hat{J}_f\hat{\mathcal{T}}]^{1/2} (-1)^{J_f - M_f + M'} \begin{pmatrix} \mathcal{G} & J_i & J_f \\ M_f - M_i & M_i & -M_f \end{pmatrix} \\ \times \begin{pmatrix} L & L' & \mathcal{G} \\ -M & M' & M_i - M_f \end{pmatrix} (-1)^{1+\Lambda} \begin{pmatrix} 1 & 1 & \mathcal{T} \\ \Lambda & -\Lambda' & \Lambda_i - \Lambda_f \end{pmatrix} Y_{L'M'}^*(\hat{k}') Y_{LM}(\hat{k}) U_{L'L}^{f\mathcal{G}\mathcal{T}}(k', k), \quad (6)$$

where

$$U_{L'L}^{f\mathcal{G}\mathcal{T}}(k', k) = \sum_{i'IKS} I_{i'IKS}^{f\mathcal{G}\mathcal{T}}(k', k) H_{i'IKS}^{L'L\mathcal{G}\mathcal{T}}(k', k). \quad (7)$$

In Eq. (7) the π -nucleus interaction is expressed as a sum of products of two factors, the first of which contains the nuclear transition form factor while the second contains the πN interaction matrix elements. Explicitly the nuclear term is

$$I_{i'IKS}^{f\mathcal{G}\mathcal{T}}(k', k) = \int_0^\infty j_{i'}(k'r) F_{i'IKS}^{f\mathcal{G}\mathcal{T}}(r) j_i(kr) r^2 dr, \quad (8)$$

where the $j_i(kr)$ are spherical Bessel functions and

$$F_{i'IKS}^{f\mathcal{G}\mathcal{T}}(r) = \sum_{\alpha\beta} \langle J_f T_f \Lambda_f | [b_\alpha^\dagger \times h_\beta^\dagger]_{\mathcal{G}\mathcal{T}} | J_i T_i \Lambda_i \rangle (4\pi j_\alpha)^{1/2} \langle \alpha | [Y_K(\hat{r}) \times \sigma_S]_{\mathcal{G}} | \beta \rangle R_{n_\alpha i_\alpha}(r) R_{n_\beta i_\beta}(r). \quad (9)$$

The operators b_α^\dagger and h_β^\dagger create, respectively, a particle or hole with shell-model quantum numbers $(n l j) \alpha$. The reduced matrix elements in Eq. (9) are defined with the convention of Brink and Satchler.⁶ The radial wave functions R_{ni} are chosen to be positive near the origin.

The factor containing the πN interaction matrix elements is

$$H_{i'IKS}^{L'L\mathcal{G}\mathcal{T}}(k', k) = i^{i'-1} (\hat{K})^{1/2} \hat{I} \hat{I}' \begin{pmatrix} l & l' & K \\ 0 & 0 & 0 \end{pmatrix} \sum_\lambda (\hat{\lambda})^{3/2} (-1)^{\lambda - \mathcal{G}} \begin{pmatrix} L' & l' & \lambda \\ 0 & 0 & 0 \end{pmatrix} \begin{pmatrix} L & l & \lambda \\ 0 & 0 & 0 \end{pmatrix} \begin{pmatrix} L & L' & \mathcal{G} \\ \lambda & \lambda & S \\ l & l' & K \end{pmatrix} \\ \times \sum_I \hat{I} (-1)^I (-1/2)^{I-1/2} \left\{ \begin{matrix} 1 & 1 & \mathcal{T} \\ \frac{1}{2} & \frac{1}{2} & I \end{matrix} \right\} t_S^{\lambda I}(k', k, W_0), \quad (10)$$

where in addition to the $9J$ symbol, the curly bracket is a simple $6J$ symbol. Thus the definition of the π -nucleus interaction potential in terms of the nuclear transition density and the πN interaction is given explicitly by Eqs. (6) through (10).

The steps in carrying out the calculation are first to separate out the angular dependence of the distorted waves as

$$\chi_{\vec{k}_0 \Lambda}^{(+)}(\vec{k}) = \sum_{LM} \chi_{L\Lambda k_0}^{(+)}(k) Y_{LM}^*(\hat{k}) Y_{LM}(\hat{k}_0). \quad (11)$$

Then to obtain the elastic optical potential, we neglect the spin-dependence of the π - N interaction and keep only the term $\mathcal{J}=0$ in evaluating Eq. (6) for $f=i$. This gives

$$U_{ii}(\vec{k}' \Lambda, \vec{k} \Lambda E) = \sum_{LM} U_{L\Lambda}(k, k', E) Y_{LM}(\hat{k}) Y_{LM}^*(\hat{k}'), \quad (12)$$

where

$$U_{L\Lambda} = \sum_{\mathcal{T}} [\hat{L} \hat{\mathcal{T}}]^{1/2} (-1)^{L+\Lambda+1} \begin{pmatrix} 1 & 1 & \mathcal{T} \\ \Lambda & -\Lambda & 0 \end{pmatrix} \times U_{LL}^{i\mathcal{J}\mathcal{T}}(k', k). \quad (13)$$

For $\mathcal{J}=0=S$, the particle-hole operators in Eq. (9) are just number operators for neutrons and protons and the nuclear factor Eq. (8) involves

integrals over the density. For the $1p$ shell we have

$$\sqrt{2} I_{i100}^{i100}(k, k) = \int_0^\infty [(A-4)R_{1p}^2(r) + 4R_{0s}^2(r)] \times j_l^2(kr) r^2 dr, \quad (14)$$

$$\sqrt{2} I_{i100}^{i101}(k, k) = 2\Lambda_i \int_0^\infty R_{1p}^2(r) j_l^2(kr) r^2 dr.$$

The $U_{L\Lambda}$ of Eq. (13) are thus related to the optical potential which is constructed in the program PIPIT by using the Gaussian ground state density determined from electron scattering. The integral equation which determines the radial distorted waves is obtained from Eqs. (2), (11), and (12) as

$$\chi_{L\Lambda k_0}^{(+)}(k) = \left(\frac{1}{k_0}\right)^2 \delta(k - k_0) + \frac{T_{L\Lambda}^{(+)}(k, k_0, E)}{E - E_\pi(k) - E_A(k) \pm i\epsilon}, \quad (15)$$

with the half-off-shell t matrix given by

$$T_{L\Lambda}^{(+)}(k, k_0, E) = \int_0^\infty k'^2 dk' U_{L\Lambda}(k, k', E) \chi_{L\Lambda k_0}^{(+)}(k'). \quad (16)$$

The final step is to obtain the transition matrix for inelastic scattering with these distorted waves

$$T_{fi}(\vec{k}'_0 \Lambda', \vec{k}_0 \Lambda) = \sum_{L'M'LM\mathcal{J}\mathcal{T}} [\hat{L} \hat{L}' \hat{J}_f \hat{\mathcal{T}}]^{1/2} Y_{L'M'}^*(k'_0) Y_{LM}(k_0) T_{L'L\Lambda'\Lambda}^{fi\mathcal{J}\mathcal{T}}(k'_0, k_0) \times (-1)^{J_f - M_f + M'} \begin{pmatrix} L & L' & \mathcal{J} \\ -M & M' & M_i - M_f \end{pmatrix} \begin{pmatrix} \mathcal{J} & J_i & J_f \\ M_f - M_i & M_i & -M_f \end{pmatrix} (-1)^{1+\Lambda} \begin{pmatrix} 1 & 1 & \mathcal{T} \\ \Lambda & -\Lambda' & \Lambda_i - \Lambda_f \end{pmatrix}, \quad (17)$$

where

$$T_{L'L\Lambda'\Lambda}^{fi\mathcal{J}\mathcal{T}}(k'_0, k_0) = \int_0^\infty k_1^2 dk_1 \int_0^\infty k_2^2 dk_2 \chi_{L'\Lambda'k'_0}^{(-)*}(k_1) U_{L'L}^{fi\mathcal{J}\mathcal{T}}(k_1, k_2) \chi_{L\Lambda k_0}^{(+)}(k_2). \quad (18)$$

The numerical methods for calculating the distorted waves and evaluating the integral of Eq. (18) have been discussed in Ref. 1. Cross sections are obtained from transition amplitudes in standard fashion.

The above formalism shows explicitly the connection of the shell model description of nuclear excitation to the DWIA calculation. Thus we can explore pion inelastic scattering on $1p$ -shell targets using the shell model of Ref. 2.

III. SHELL-MODEL TRANSITION DENSITIES

The nuclear structure input to the DWIA calculation is contained in Eq. (9). The LS representation, wherein the particle-hole spins are coupled to S and the l 's to K , simplifies the expression for F in our $1p$ -shell cases and is also the clearest way to relate the F 's to matrix elements for electromagnetic transitions. In the LS representation

$$F_{KS}^{fi\mathcal{J}\mathcal{T}}(r) = \sum_{\alpha\beta} \langle J_f T_f \Lambda_f || [b_{(ni)\alpha}^\dagger \times h_{(ni)\beta}^\dagger] g_{(KS)\mathcal{T}} || J_i T_i \Lambda_i \rangle (2\hat{\mathcal{J}} \hat{l}_\alpha \hat{l}_\beta)^{1/2} (-1)^l \alpha \begin{pmatrix} l_\alpha & l_\beta & K \\ 0 & 0 & 0 \end{pmatrix} R_{n_\alpha l_\alpha}(r) R_{n_\beta l_\beta}(r). \quad (19)$$

For the $1p$ shell there is no summation since all the active nucleons are $1p$ nucleons, and only even values

of K give nonzero F values.

For electromagnetic transitions wherein the single-particle matrix element is

$$\langle \alpha t_3 | Q_g | \beta t_3 \rangle = \gamma_{t_3} \langle \alpha | f_K(r) [Y_K \times \sigma_S]_g | \beta \rangle,$$

TABLE I. Transition density amplitudes $A_{J(KS)}$ for neutrons and protons in $1p$ -shell targets. For mass 6 to 9 the (6-16)2B interaction of Ref. 2 is used and the (8-16)POT interaction for larger mass. For $T=0$ targets only the neutron amplitude is given since the proton amplitude is $(-1)^{T_f}$ times the neutron value. For each target final state JT values are given in the first column where an asterisk labels the second state of same JT . The remaining columns are labeled by $J(KS)$ as in Eq. (21).

$(J_f T_f)$	t_3	3(21)	2(21)	2(11)	2(20)	1(21)	1(11)	1(01)	1(10)	0(11)	0(00)
${}^6\text{Li}(1, 0)$											
(01)	n					0.191	-0.015	0.678	0.060		
(10)	n		0	-0.089	0.239	-0.096	0	0.507	0.043	0.010	0.408
(10)*	n		0.479	0.053	-0.427	0.078	0.008	0.232	-0.142	-0.134	0
(20)	n	-0.421	0.271	-0.094	-0.302	0.353	0.117	-0.108	0.066		
(21)	n	0.478	0.314	-0.034	-0.034	0.358	-0.154	0.081	-0.096		
(30)	n	0.437	0.355	-0.027	0.416						
${}^7\text{Li}(\frac{3}{2}, \frac{1}{2})$											
$(\frac{1}{2} \frac{1}{2})$	n		-0.032	0.082	1.088	0.016	-0.005	0.008	0.284		
	p		-0.655	-0.203	0.543	-0.215	-0.284	-0.658	0.114		
$(\frac{3}{2} \frac{1}{2})$	n	0.009	0	0.074	0.748	-0.057	0	0.005	0.381	-0.107	0.816
	p	0.844	0	0.350	0.400	-0.140	0	0.525	0.262	-0.129	0.408
$(\frac{3}{2} \frac{3}{2})^*$	n	-0.339	0.381	0.003	-0.046	-0.297	0.425	0.054	0.087	-0.236	0
	p	-0.171	-0.029	-0.129	-0.084	0.021	0.017	-0.006	-0.116	0.077	0
$(\frac{5}{2} \frac{3}{2})$	n	-0.384	0.055	-0.509	-0.242	0.125	-0.094	-0.003	-0.285	0.066	0
	p	0.384	-0.055	0.509	0.242	-0.125	0.094	0.003	0.285	-0.066	0
$(\frac{5}{2} \frac{1}{2})$	n	0.194	-0.019	0.211	-0.317	-0.022	-0.185	-0.019	0.034		
	p	0.118	0.311	-0.003	-0.174	0.375	-0.004	0.002	-0.024		
$(\frac{5}{2} \frac{1}{2})^*$	n	0.308	-0.153	0.686	0.166	0.036	-0.436	-0.043	-0.056		
	p	-0.115	-0.144	0.093	-0.006	-0.108	0.046	0.007	0.078		
$(\frac{7}{2} \frac{1}{2})$	n	0.096	0.007	-0.159	-0.732						
	p	-0.357	-0.268	-0.014	-0.338						
$(\frac{7}{2} \frac{1}{2})^*$	n	0.243	-0.150	-0.569	0.158						
	p	0.067	0.034	0.012	0.050						
${}^9\text{Be}(\frac{3}{2}, \frac{1}{2})$											
$(\frac{1}{2} \frac{1}{2})$	n		0.849	0.173	-0.493	0.260	0.437	0.619	-0.243		
	p		0.008	-0.091	0.227	-0.009	0.035	0.007	-0.140		
$(\frac{3}{2} \frac{1}{2})$	n	1.031	0	-0.039	-0.357	-0.221	0	0.433	0.514	-0.453	1.225
	p	0.034	0	-0.118	-0.646	-0.030	0	0.003	0.188	-0.191	0.817
$(\frac{3}{2} \frac{3}{2})$	n	-0.313	-0.053	0.431	0.221	0.033	-0.179	-0.045	-0.197	-0.021	0
	p	0.313	0.053	-0.431	-0.221	-0.033	0.179	0.045	0.197	0.021	0
$(\frac{5}{2} \frac{1}{2})$	n	-0.318	0.126	0.400	-0.789	-0.092	0.224	0.157	0.161		
	p	0.039	0.021	-0.159	-0.876	0.028	-0.006	-0.009	-0.252		
$(\frac{7}{2} \frac{1}{2})$	n	-0.361	-0.096	-0.026	0.272						
	p	0.118	-0.075	0.275	0.538						
${}^{10}\text{B}(3, 0)$											
(01)	n	1.094									
(10)	n	-0.442	0.516	0.001	-0.451						
(10)*	n	-0.873	-0.235	0.339	0.197						
(20)	n	0.115	-0.382	-0.138	0.279	-0.138	-0.004	-0.174	0.107		
(20)*	n	0.127	0.064	0.108	0.189	0.103	0.389	0.345	-0.211		
(21)	n	-0.635	0.110	0.490	0.072	0.164	0.126	0.147	-0.200		
(21)*	n	0.404	0.223	-0.058	-0.108	0.075	0.361	0.399	-0.026		
(30)	n	0.284	0	-0.010	-0.761	-0.275	0	0.387	0.629	-0.559	1.225
(30)*	n	0.396	-0.207	-0.352	0.268	-0.022	0.075	-0.004	0.002	-0.031	0
(40)	n	-0.151	-0.258	-0.351	0.665	0.124	-0.284	-0.160	0.098		

TABLE I. (Continued.)

$(J_f T_f)$	t_3	3(21)	2(21)	2(11)	2(20)	1(21)	1(11)	1(01)	1(10)	0(11)	0(00)
$^{11}\text{B}(\frac{3}{2}, \frac{1}{2})$											
$(\frac{1}{2} \frac{1}{2})$	n		-0.101	-0.150	0.788	0.009	-0.045	-0.011	-0.037		
	p		-0.803	0.101	0.397	-0.326	-0.098	-0.541	0.375		
$(\frac{1}{2} \frac{3}{2})$	n		-0.310	-0.170	0.363	-0.030	-0.410	-0.153	-0.033		
	p		0.310	0.170	-0.363	0.030	0.410	0.153	0.033		
$(\frac{3}{2} \frac{1}{2})$	n	0.018	0	0.138	-0.316	0.022	0	0.006	0.174	-0.511	1.633
	p	1.040	0	-0.537	-0.685	-0.367	0	0.329	0.590	-0.545	1.225
$(\frac{3}{2} \frac{3}{2})^*$	n	0.056	-0.126	-0.133	0.605	-0.055	0.030	-0.003	-0.152	-0.030	0
	p	0.391	0.014	-0.180	0.203	0.233	0.552	0.360	-0.067	0.162	0
$(\frac{5}{2} \frac{1}{2})$	n	0.029	-0.104	-0.243	0.506	0.014	0.072	0.027	-0.045		
	p	0.145	-0.433	-0.403	0.779	0.130	-0.332	-0.252	0.183		
$(\frac{7}{2} \frac{1}{2})$	n	0.060	0.258	0.226	-0.722						
	p	0.040	-0.239	-0.077	-0.236						
$^{12}\text{C}(0, 0)$											
(00)	n									-0.497	1.633
(10)	n					-0.049	-0.537	-0.152	0.093		
(11)	n					0.096	0.515	0.160	-0.023		
(20)	n		0.129	0.185	-0.641						
(21)	n		-0.283	-0.264	0.299						
$^{13}\text{C}(\frac{1}{2}, \frac{1}{2})$											
$(\frac{1}{2} \frac{1}{2})$	n					0.929	0	-0.235	0.464	-0.463	2.041
	p					0.039	0	-0.003	0.115	-0.739	1.633
$(\frac{1}{2} \frac{3}{2})^*$	n					-0.071	0.014	-0.020	-0.062	0.074	0
	p					0.135	0.761	0.293	-0.105	0.151	0
$(\frac{3}{2} \frac{1}{2})$	n		0.552	0.261	-0.435	-0.198	-0.316	-0.428	0.186		
	p		0.182	0.250	-0.629	0.010	0.005	0.017	0.065		
$(\frac{3}{2} \frac{3}{2})$	n		-0.364	-0.247	0.352	0.097	0.403	0.162	-0.101		
	p		0.364	0.247	-0.352	-0.097	-0.403	-0.162	0.101		
$(\frac{5}{2} \frac{1}{2})$	n	-0.023	-0.156	0.047	-0.157						
	p	0.036	0.362	0.330	-0.692						
$(\frac{7}{2} \frac{1}{2})$	n	-0.229									
	p	0.056									
$^{14}\text{N}(10)$											
(01)	n					-1.013	0.080	0.109	-0.423		
(10)	n		0	0.117	-0.188	0.755	0	-0.257	0.511	-0.554	2.041
(10)*	n		-0.553	-0.206	0.451	0.301	0.182	0.086	-0.052	-0.063	0
(11)	n		0.532	0.255	-0.503	-0.070	-0.274	-0.125	0.186	0.090	0
(20)	n	0.106	-0.391	-0.314	0.334	0.101	0.412	0.368	-0.225		
(21)	n	0.097	-0.430	-0.271	0.260	0.245	0.436	0.325	-0.128		
(30)	n	0.059	-0.090	-0.076	0.056						
$^{15}\text{N}(\frac{1}{2}, \frac{1}{2})$											
$(\frac{1}{2} \frac{1}{2})$	p					1.054	0	-0.236	0.577	-0.577	2.041
$(\frac{3}{2} \frac{1}{2})$	p		0.791	0.456	-0.646	-0.264	-0.612	-0.471	0.289		

the reduced matrix element is

$$\begin{aligned}
\langle J_f T_f \Lambda \| Q_{\mathcal{G}}(K \times S) \| J_i T_i \Lambda \rangle = & \sum_{\mathcal{T}} [\gamma_n + (-1)^x \gamma_p] \sum_{\alpha\beta} \langle J_f T_f \Lambda \| b_{(n)\alpha}^\dagger \times h_{(n)\beta}^\dagger \|_{\mathcal{G}(KS)\mathcal{T}} \| J_i T_i \Lambda \rangle \\
& \times \left(\frac{\hat{l}_\alpha \hat{l}_\beta}{4\pi} \right)^{1/2} (-1)^l \alpha \begin{pmatrix} l_\alpha & l_\beta & K \\ 0 & 0 & 0 \end{pmatrix} \langle R_{n\alpha} | f_K(r) | R_{n\beta} \rangle. \quad (20)
\end{aligned}$$

The quantities γ_n, γ_p would be magnetic moments of neutron and proton in magnetic transitions or effective charges in electric-transitions.

The reduced matrix element of the particle-hole operator between initial and final nuclear states, called the transition density, is a factor common to Eqs. (19) and (20). Numerical values for these quantities have been calculated for the $1p$ shell using the interactions of Cohen and Kurath in the Argonne shell-model program.⁷ For pion scattering it is useful to know the separate contributions from neutron and proton transitions, so the quantities listed in Table I are matrix elements

$$\langle J_f T_f || [b_{t_3}^\dagger \times \bar{b}_{t_3}]_{g(KS)} || J_i T_i \rangle \equiv A_{g(KS)t_3} \quad (21)$$

evaluated for $\Lambda = T_i$. Here the hole operator is related to the usual destruction operator by

$$\bar{b}_{t_3} s_{z t_3} = (-1)^{1/2 - t_3 - s_z} b_{-t_3} - s_{z t_3}. \quad (22)$$

The amplitudes of Eq. (21) are simply related to those of the transition density in Eq. (20) since for a given (KS)

$$\sqrt{2} [b_{t_3}^\dagger \times \bar{b}_{t_3}] = [b^\dagger \times h^\dagger]_{T=0} + 2t_3 [b^\dagger \times h^\dagger]_{T=1}. \quad (23)$$

Some of these operators represent simple quantities; for example $K=0=S$ is just $6^{-1/2}$ times the operator for the number of $1p$ nucleons with a given t_3 .

In comparing calculated values for Gamow-Teller beta decays and $M1$ transitions with observation, reasonable overall agreement is found in the $1p$ shell when free nucleon moments are used in the $M1$ cases. For $E2$ transitions ($K=2, S=0$), however, calculated $B(E2)$ values are often too small by factors ranging from 2 to 6. This is because quadrupole deformation is not adequately described within the $1p$ space, and the enhancement needed can be calculated⁸ by going outside the $1p$ shell. The effect can be included by using effective charges, or alternatively, as one sees from Eq. (20), enhancing the pertinent transition density matrix element. We shall show that similar enhancement is needed to fit inelastic pion scattering to such states.

Finally, the radial functions R_{1p} are chosen to be oscillator functions with oscillator parameter $b = 1.67$ fm. This value is commonly used in calculating the radial dependence for $E2$ gamma transitions in the $1p$ shell.

IV. NUMERICAL RESULTS AND COMPARISON WITH DATA

A. Elastic scattering

In determining the optical potential for elastic scattering by means of the PIPIT program,⁵ the

Gaussian ground state density contains an adjustable range parameter b . Figure 1 contains the data⁹ for elastic π^- scattering on ^{12}C at 162 MeV and the solid curve which results from calculation with a parameter value of $b = 1.67$ fm as suggested by electron scattering. A much better fit can be obtained by choosing $b = 1.40$ fm which gives the dash-dot curve in Fig. 1. A similar behavior has been noted for other nuclei,²⁰ and while it is likely due to higher order effects in the density, it should be viewed at present as simply a way to determine a phenomenological optical potential. We use $b = 1.40$ fm for getting the elastic optical potential in all $1p$ -shell nuclei.

B. Quadrupole dominance of inelastic scattering

Upon surveying our calculations of inelastic scattering we find that the strong transitions in the $1p$ shell have a special property. In all such cases there are relatively strong amplitudes in Table I which have $(KS) = (20)$. Furthermore, if one applies the collective model to interpret the $1p$ spectra, all the final states which show strong

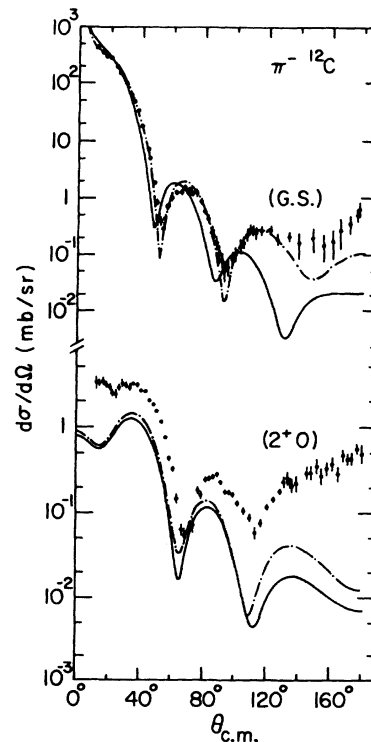


FIG. 1. The differential cross sections for 162 MeV π^- scattering to the ground state and the 4.44 MeV (2^+0) state in ^{12}C . The solid (dash-dot) curves are calculated by using the optical potential with oscillator parameter $b = 1.67$ (1.4) fm. No enhancement factor is included to evaluate the transition form factor. The data are from Ref. 9.

transitions are members of the same rotational band as the ground state. An example is the excitation of the $J=2$ first excited state of ^{12}C shown at the bottom of Fig. 1. The (20) amplitude in Table I is clearly dominant and this is by far the largest cross section we calculate for ^{12}C . Nevertheless, although the calculated shape resembles the data, we see from Fig. 1 that the calculated magnitude is too small by a factor of about 2.

It has long been known that a similar discrepancy with experiment exists for $E2$ transitions calculated with $1p$ wave functions. If one calculates the $B(E2)$ value between these ^{12}C states with the same oscillator parameter, $b=1.67$ fm, used in our inelastic pion cross-section calculation, the result is also a factor of 2 smaller than experiment.

This comparison suggests that for such states replacing $A_{(20)}$ by $EA_{(20)}$, with E determined by the $B(E2)$ comparison, will lead to the observed magnitude for (π, π') scattering. In Table II we list the states contained in the ground-state rotational bands and the enhancement factors consistent with observed $B(E2)$ transitions for $T=0$ targets. Since these are all isoscalar transitions we assume the same E values for neutrons as for protons. The band members are identified as those leaving the same intrinsic spatial wave function labeled by K_0 , the projection of orbital angular momentum on the nuclear symmetry axis. There have been calculations^{8,10} of E values by using the Nilsson model to extend beyond the $1p$ -shell space. The results are in rough agreement with observations, but our procedure is to select a single enhancement factor for all transitions in a band, usually based on an average value for observed $E2$ transitions within the band.

For transitions in odd- A nuclei we need enhancement factors for both neutrons and protons. In these $T=\frac{1}{2}$ nuclei the bands arise from intrinsic states labeled by J_0 , the projection of total angular momentum on the nuclear symmetry axis. The states involved and our selected enhancement factors are given in Table III. In ^{11}B the bands are

TABLE II. Enhancement factors for $T=0$ targets. Bands are identified by the projection K_0 of orbital angular momentum on the nuclear symmetry axis. Band members are given in column 3, and column 4 gives the enhancement factors for the $(KS)=(20)$ amplitudes assuming $E_n=E_p$.

Target	K_0	States	$E_n=E_p$
^6Li	0	(1, 1*, 2, 3)	2.5
^{10}B	2	(3, 4)	2.0
^{12}C	0	(0, 2)	1.4
^{14}N	0	(1, 1*, 2, 3)	1.7

TABLE III. Enhancement factors for $T=\frac{1}{2}$ targets. Bands are identified by the projection of total angular momentum on the nuclear symmetry axis. Band members are given in column 3. Neutron and proton factors for $(KS)=(20)$ amplitudes are in the last two columns.

Target	J_0	States	E_n	E_p
^7Li	$\frac{1}{2}$	$(\frac{3}{2}, \frac{1}{2}, \frac{5}{2}, \frac{7}{2})$	1.75	2.5
^9Be	$\frac{3}{2}$	$(\frac{3}{2}, \frac{5}{2}, \frac{7}{2})$	2.4	1.75
^{11}B	$\frac{3}{2}$	$(\frac{3}{2}, \frac{5}{2}, \frac{7}{2})$	1.4	1.6
	$\frac{1}{2}$	$(\frac{1}{2}, \frac{3}{2}, \frac{5}{2}, \frac{7}{2})$	1.4	1.6
^{13}C	$\frac{1}{2}$	$(\frac{1}{2}, \frac{3}{2}, \frac{5}{2})$	2.1	1.4
^{15}N	$\frac{1}{2}$	$(\frac{1}{2}, \frac{3}{2})$		1.25

strongly mixed so all the states listed are expected to have some enhancement. We again select one pair of enhancement factors for each nucleus, taken mainly from $B(E2)$ comparisons wherein the number of protons is equal to the appropriate number of nucleons. For example, the E_n value for ^7Li is taken as equal to the E_p value in ^9Be . The E_n values for ^9Be and ^{13}C are larger than the general trend due to the structure of the intrinsic states. For ^9Be the intrinsic state is prolate except for the odd neutron which is in an oblate orbital and thus makes a contribution of opposite sign to the other neutrons when the $(KS)=(20)$ matrix element is evaluated. However, when this matrix element is evaluated in the enlarged space the effect is to reduce the contribution of the odd nucleon, so the net effect is a bigger than average enhancement factor. A similar explanation applies to ^{13}C where the intrinsic state is oblate but the last neutron is in a prolate orbital.

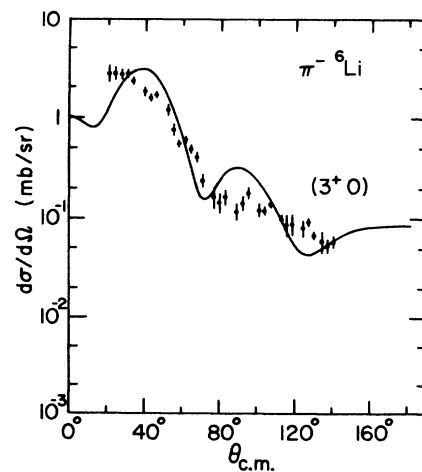


FIG. 2. The differential cross sections for 164 MeV π^- scattering to the 2.185 MeV (3^+0) state in ^6Li . The data are from Ref. 11.

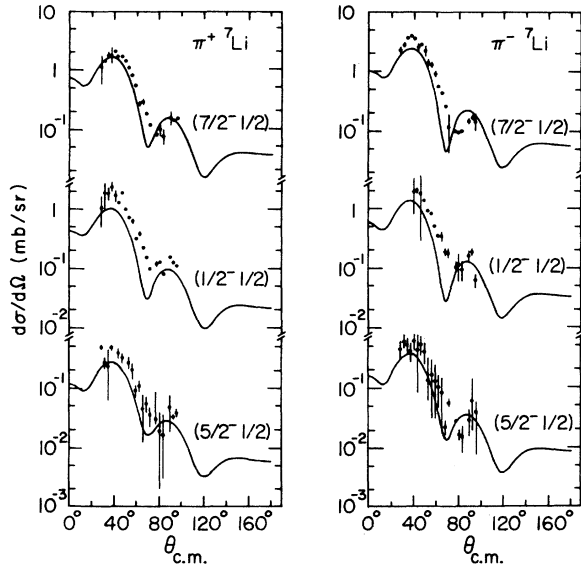


FIG. 3. The differential cross sections for 164 MeV π^+ scattering to the 0.478 MeV ($\frac{1}{2}^- \frac{1}{2}$), 4.63 MeV ($\frac{1}{2}^- \frac{1}{2}$), and 6.68 MeV ($\frac{5}{2}^- \frac{1}{2}$) states in ${}^7\text{Li}$. The data are from Ref. 12.

The use of E_N and E_P factors for the $(KS) = (20)$ amplitudes is a substitute for doing much more complex Hartree-Fock calculations in an enlarged model space. There may be more detailed data in the future which will then warrant such an effort, but for now our procedure seems suited to the existing data.

C. Comparison with data

In Fig. 2 the data¹¹ for exciting the $J = 3^+$ state of ${}^6\text{Li}$ by π^- beams at 162 MeV are compared to

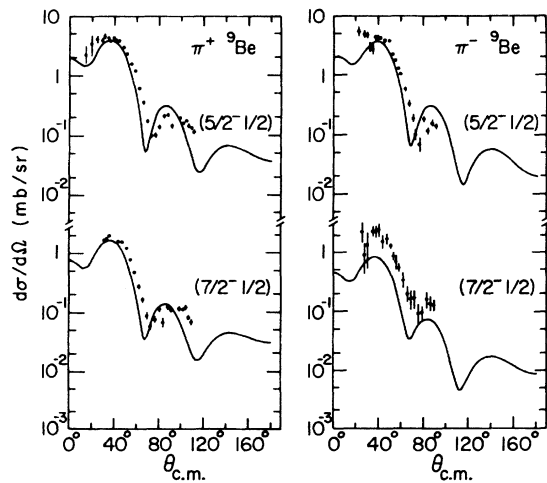


FIG. 4. The differential cross sections for 162 MeV π^+ scattering to the 2.429 MeV ($\frac{5}{2}^- \frac{1}{2}$) and 6.76 MeV ($\frac{7}{2}^- \frac{1}{2}$) states in ${}^9\text{Be}$. The data are from Ref. 13.

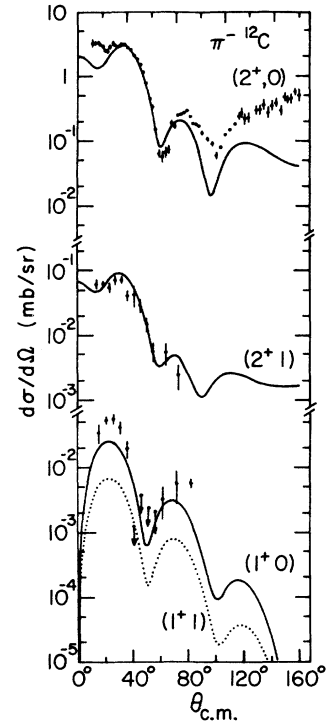


FIG. 5. The differential cross sections for 162 MeV π^- scattering to the 4.44 MeV ($2^+ 0$) state in ${}^{12}\text{C}$ (data from Ref. 9) and for 180 MeV π^+ scattering to the 16.11 MeV ($2^+ 1$) and 12.71 MeV ($1^+ 0$) states (data from Ref. 14). The calculated result for the 15.11 MeV ($1^+ 1$) state is the dotted curve.

our calculation, and in Fig. 3 excitation¹² of the rotational band members of ${}^7\text{Li}$ by π^+ beams at 164 MeV is compared to calculation. Agreement is reasonably good, particularly for the relative

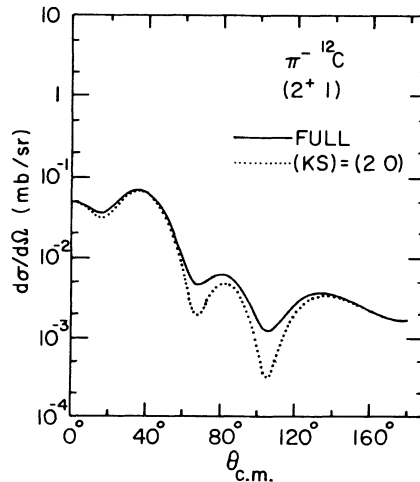


FIG. 6. The differential cross sections for 162 MeV π^- scattering to the 16.11 MeV ($2^+ 1$) state ${}^{12}\text{C}$. The dashed curve is calculated by using only the transition form factor of $(KS) = (2 0)$ (see Table I).

values to different states of ${}^7\text{Li}$. The enhancement factors taken from $B(E2)$ comparisons are clearly needed to obtain such agreement.

In Fig. 4 excitation¹³ of the $J = \frac{5}{2}^-$ and $\frac{7}{2}^-$ rotational band members of ${}^9\text{Be}$ is compared to calculations for both π^+ and π^- beams at 162 MeV. The calculated cross section for π^- scattering to the $\frac{7}{2}$ state is low by a factor of 2, but the other three cases show good agreement.

In Fig. 5 inelastic scattering of π^+ beams on ${}^{12}\text{C}$ is treated. The data for exciting the rotational 2^+ $T=0$ level agree well with the calculation for 162 MeV pions, now including an enhancement factor. The other cases involve excitation of states where there should be no enhancement. The calculated cross sections, when compared to this 180 MeV data,¹⁴ show good agreement for the 2^+ $T=1$ level at 16 MeV and a somewhat low calculated value for the 1^+ $T=0$ level at 12.7 MeV. The calculated cross section for exciting the $J=1^+$ $T=1$ level at 15.1 MeV is included with the 12.7 MeV case in Fig. 5. From Table I one sees that the $(KS) = (01)$ amplitudes, which are dominant in the calculation, are nearly equal for these two states. Therefore, one expects a cross-section ratio of nearly 4 to 1 favoring transition to the $T=0$ state, as is found in the calculations. It is known that there is a small amount of isospin mixing between these states as discussed by Adelberger *et al.*¹⁵ These authors determine, based mainly on the $B(M1)$ of the 12.7 MeV state, that the admixture amplitude is about 0.05. The sign of this admixture is such that the calculated cross-section ratio becomes 3.2 to 1 for π^- scattering and 5.2 to 1 for π^+ scattering instead of 4 to 1 for each if there were no isospin mixing. Pion scattering offers a very sensitive way to determine isospin mixing.

The calculated excitation of the 2^+ $T=1$ state is presented in Fig. 6 to show the dominance of the $(KS) = (20)$ component in the πN interaction. Although the two contributing amplitudes with $(KS) = (21)$ and (20) are seen to be nearly equal from Table I, the cross section is seen to be mainly due to (20) with (21) mainly filling in the minima at larger angles.

Although our data comparison is comprised mainly of the strong rotational band members, there are other states in the case of ${}^{12}\text{C}$. The degree of agreement is sufficiently encouraging to warrant presentation of the calculated cross sections for all $1p$ -shell targets.

D. Calculated cross-section predictions

In Figs. 7–13 we give calculated cross sections for π^+ inelastic scattering at 162 MeV to low-lying normal parity states in the $1p$ shell. Results

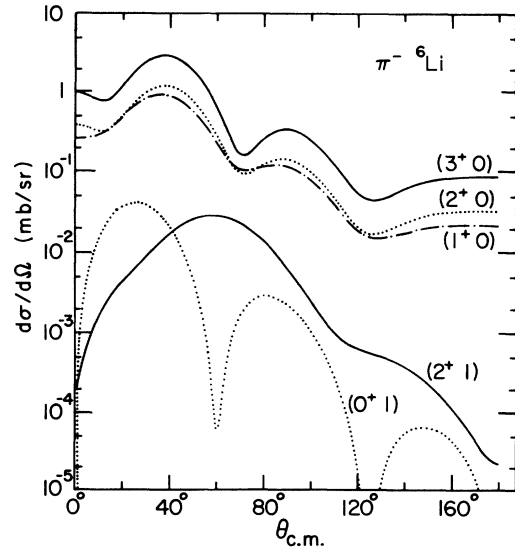


FIG. 7. The calculated differential cross sections for 162 MeV π^- scattering to the states: (a) 2.185 MeV (3^+ 0), (b) 3.563 MeV (0^+ 1), (c) 4.31 MeV (2^+ 0), (d) 5.37 MeV (2^+ 1), and (e) 5.65 MeV (1^+ 0) in ${}^6\text{Li}$.

for ${}^9\text{Be}$ and ${}^{12}\text{C}$ have already been given in the data comparison so they are not repeated. A common feature in these curves is the dominance of scattering to rotational band members. This is due in part to our inclusion of enhancement factors, but since the latter only provide a factor between 2 and 6 to the magnitude, scattering to these particular states would be dominant even without enhancement factors.

${}^6\text{Li}$. Transitions to (20) , (21) , and $(10)^*$ may be difficult experimentally since these are broad overlapping states around 4 to 5 MeV.

${}^7\text{Li}$. The strong π^+ cases agree well with experiment in Fig. 3. The π^- cross sections to these states are calculated to be about 1.5 times the π^+ cross sections. There is another effective inter-

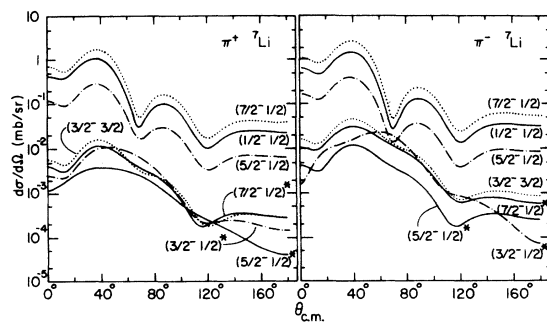


FIG. 8. The calculated differential cross sections for 162 MeV π^+ scattering to the states: (a) 0.48 MeV ($\frac{3}{2}^- \frac{3}{2}$), (b) 4.63 MeV ($\frac{7}{2}^- \frac{1}{2}$), (c) 6.68 MeV ($\frac{1}{2}^- \frac{1}{2}$), (d) 7.46 MeV ($\frac{5}{2}^- \frac{1}{2}$)*, (e) 9.67 MeV ($\frac{7}{2}^- \frac{1}{2}$)*, (f) 9.9 MeV ($\frac{3}{2}^- \frac{1}{2}$)*, and (g) 11.24 MeV ($\frac{5}{2}^- \frac{1}{2}$)* in ${}^7\text{Li}$.

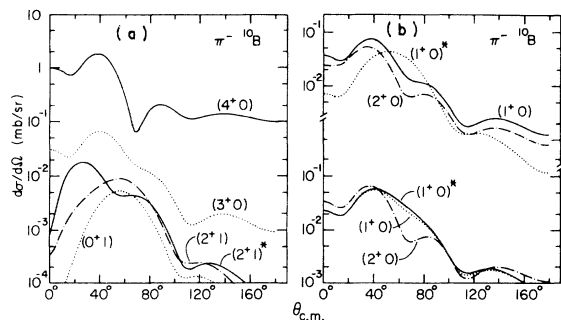


FIG. 9. The calculated differential cross sections for 162 MeV π^- scattering to the excited states in ^{10}B . The excited states in (a) are (a) 1.74 MeV (0^+1), (b) 4.774 MeV (3^+0), (c) 6.025 MeV (4^+0), (d) 5.164 MeV (2^+1), and (e) 7.48 MeV (2^+1) * states. The excited states in (b) 0.718 MeV (1^+0) * , 2.154 MeV (1^+0) * , and 3.58 MeV (2^+0) states. The curves in the upper and lower parts of (b) are calculated by using different nuclear wave functions as discussed in Sec. IV.

action for light nuclei determined by Kumar¹⁶ by fitting nuclear spectra from $A=6$ to $A=9$. Cross sections calculated with Kumar's interaction are very close to our results for the strong rotational band members and for the $\frac{3}{2}$, $T=\frac{3}{2}$ state at 11 MeV. However, for the weak transitions to the $\frac{3}{2}^*$, $\frac{5}{2}^*$, and $\frac{7}{2}^*$ states, our results show some considerable differences from results using Kumar's interaction, though the transitions are not reliable since the (6-16)2B interaction is not suitable here.

^{10}B . In this nucleus only the transition to the $J=4$ state at 6 MeV is predicted to be strong. Transitions to the $T=1$ states are of interest since the $(KS)=(20)$ amplitudes are weak or absent. The cross sections near 60° in Fig. 9(a) are determined by the $g(KS)=3(21)$ amplitudes, while the forward peak for the second $J=2$, $T=1$ state (at 7.5 MeV) is determined by the $(KS)=(01)$ amplitude. Unfortunately these cross sections are

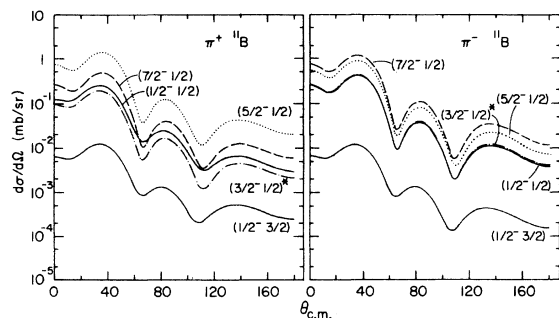


FIG. 10. The calculated differential cross sections of 162 MeV π^+ scattering to the states: (a) 2.125 MeV ($\frac{1}{2}^--\frac{1}{2}$), (b) 4.445 MeV ($\frac{5}{2}^--\frac{1}{2}$), (c) 5.021 MeV ($\frac{3}{2}^--\frac{1}{2}$) * , (d) 6.743 MeV ($\frac{7}{2}^--\frac{1}{2}$), and (e) 12.91 MeV ($\frac{1}{2}^--\frac{3}{2}$) in ^{11}B .

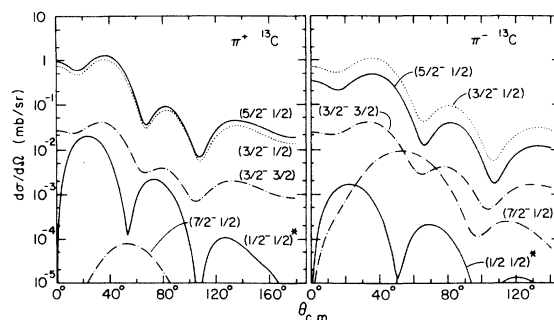


FIG. 11. The calculated differential cross sections of 162 MeV π^+ scattering to the states: (a) 3.684 MeV ($\frac{3}{2}^--\frac{1}{2}$), (b) 7.547 MeV ($\frac{5}{2}^--\frac{1}{2}$), (c) 8.86 MeV ($\frac{1}{2}^--\frac{1}{2}$) * , (d) 10.753 MeV ($\frac{7}{2}^--\frac{1}{2}$), and (e) 15.106 MeV ($\frac{3}{2}^--\frac{3}{2}$) in ^{13}C .

small, so they may be difficult to observe. In Fig. 9(b) cross sections are given for the $T=0$ states with $J=1$, 1^* , and 2 associated with levels of energies of 0.7, 2.2, and 3.6 MeV, respectively. The upper curves result from the use of the (8-16)POT interaction of Ref. 2. Warburton *et al.*¹⁷ found that they could obtain a much greater similarity to experiment for gamma transitions involving these levels by mixing the two lowest eigenfunctions for each J with 16% intensity of the upper state admixed to the lower state. The lower curves are cross sections obtained with such wave functions, and the chief effect is to make the two $J=1$ cross sections very close in shape and magnitude. Hopefully experiment will determine whether these mixed wave functions give a consistently better picture.

^{11}B . In ^{11}B the main point of interest is the dif-

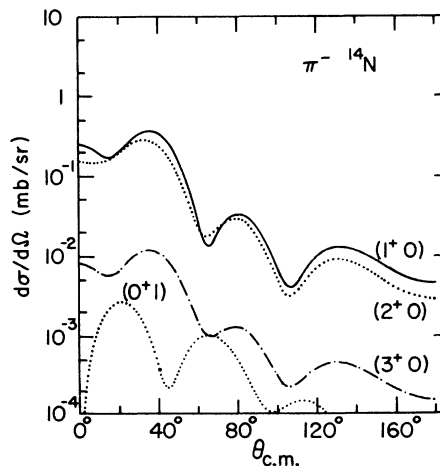


FIG. 12. The calculated differential cross sections for 162 MeV π^- scattering to the states: (a) 2.313 ($0^+,1$), (b) 3.948 MeV (1^+0) * , (c) 7.03 MeV (2^+0), and (d) 11.0 MeV (3^+0) in ^{14}N .

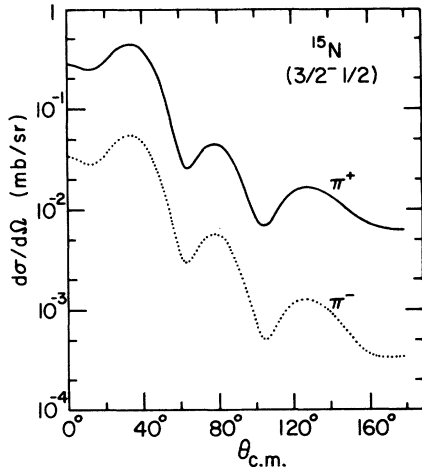


FIG. 13. The calculated differential cross sections for 162 MeV π^+ and π^- scattering to the 6.32 MeV ($\frac{3}{2}^- \frac{1}{2}$) state in ^{15}N .

ference between π^+ and π^- excitation for the strong transitions to $\frac{1}{2}$, $\frac{3}{2}^*$, $\frac{5}{2}$, and $\frac{7}{2}$ associated with the states observed at 2.1, 5.0, 4.4, and 6.7 MeV, respectively. From Fig. 10 we see that the π^- to π^+ ratios are calculated (at the first peaks) to be about 1.6, 2.1, 0.6, and 2.4, respectively. These are crude estimates since we used the same enhancement factors for all these states even though they arise from two mixed bands. Experiment can tell how good this approximation is.

^{13}C . Again the most interesting point concerns ratios of π^- to π^+ scattering as shown in Fig. 11. The strong transition to $J = \frac{3}{2}$ at 3.7 MeV shows

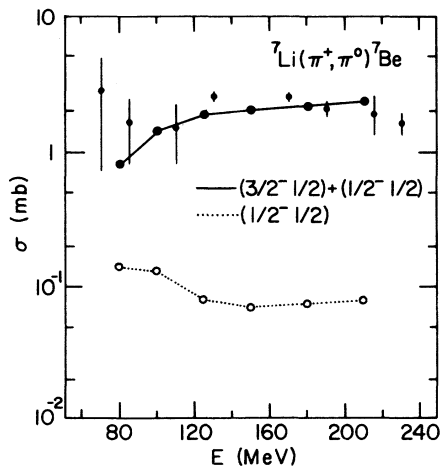


FIG. 14. Integrated cross sections for ${}^7\text{Li}(\pi^+, \pi^0){}^7\text{Be}$. The solid curve is the sum of contributions from the ($\frac{3}{2}^- \frac{1}{2}$) ground state and the ($\frac{1}{2}^- \frac{1}{2}$) state at 0.43 MeV. The dotted curve is for the latter only. Data are from Ref. 18.

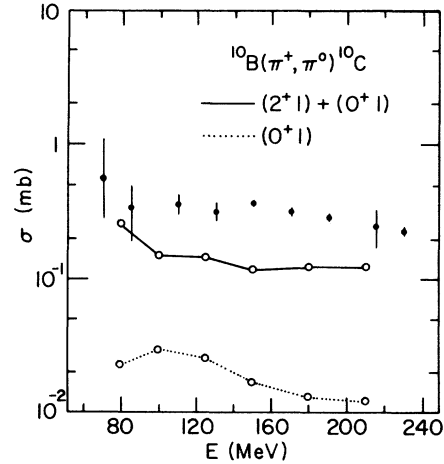


FIG. 15. Integrated cross sections for ${}^{10}\text{B}(\pi^+, \pi^0){}^{10}\text{C}$. The solid curve is the sum of contributions from the ($0^+ 1$) ground state and the ($2^+ 1$) state at 3.35 MeV. The dotted curve is for the ground state only. Data are from Ref. 18.

little difference but the strong transition to $J = \frac{5}{2}$ at 7.5 MeV favors π^+ by a factor of 2. More dramatic differences are predicted for the weak transitions to the $\frac{1}{2}^*$ at 8.9 MeV where π^+ is favored by an order of magnitude, and the $\frac{7}{2}$ state at 10.8 MeV where π^- is favored by an order of magnitude. However, observation of these ratios may be obscured by the presence of nearby levels of opposite parity as will be discussed later.

$^{14,15}\text{N}$. In ^{14}N only the $T=0$ band members, $J=1^*$ at 3.9 MeV and $J=2$ at 7.0 MeV have appreciable cross section in Fig. 12. In ^{15}N there is only the $J = \frac{3}{2}$ proton hole state at 6.3 MeV which should favor π^+ scattering as in Fig. 13.

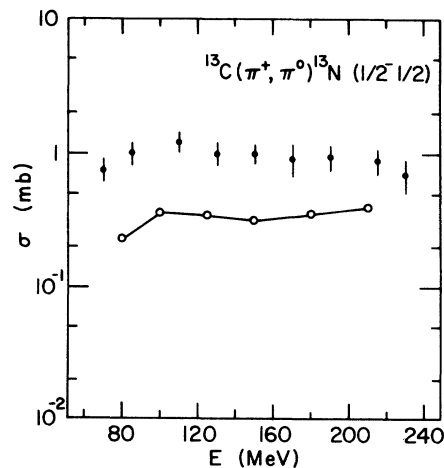


FIG. 16. Integrated cross sections for ${}^{13}\text{C}(\pi^+, \pi^0){}^{13}\text{N}$ to the ($\frac{1}{2}^- \frac{1}{2}$) ground state. Data are from Ref. 18.

E. Data comparison for (π^+, π^0) calculations

In Figs. 14 to 16 we compare calculations of the (π^+, π^0) cross sections with observation for ${}^7\text{Li}$, ${}^{10}\text{B}$, and ${}^{13}\text{C}$ in the energy range of 100 to 200 MeV. The observed cross sections¹⁸ are all nearly independent of the energy in this range, while the calculations show some small variation. Transitions to isobaric analogs of the target state are dominated by the T^- operator, and here the calculation agrees with the data in ${}^7\text{Li}$ and is lower than observed in ${}^{13}\text{C}$ by a factor of 3 to 4. Transition to the $J=\frac{1}{2}$ state of ${}^7\text{Be}$ is calculated to be a minor contribution. Transition from ${}^{10}\text{B}$ to ${}^{10}\text{C}$ is lower than observed by a factor of 2 to 3 with the calculated strength going mainly via the $J=2$ state. It is clear that our calculations fail to produce the observations for all but ${}^7\text{Li}$.

V. DISCUSSION

The major finding of our investigation of inelastic pion scattering in the $1p$ shell is the dominance of the $(KS)=(20)$ multipole in our DWIA calculation of the cross sections. Therefore, strong transitions occur to states which can be considered as belonging to the same rotation band as the ground state, and we need to use enhancement factors consistent with those required for $B(E2)$ transitions to obtain agreement with existing data. A similar feature is known for inelastic scattering with other projectiles such as protons and alpha particles. The distinctive feature of pions is that by using both π^+ and π^- beams one tests the contributions of both neutrons and protons separately.

A simple estimate of the cross section at the first forward maximum for states in which the $A_{(20)}$ amplitudes are not unusually small is given by

$$\begin{aligned} \left(\frac{d\sigma}{d\Omega}\right)_- &\simeq C(A)(\hat{J}_f/\hat{J}_i)(3E_N A_{(20)N} + E_P A_{(20)P})^2, \\ \left(\frac{d\sigma}{d\Omega}\right)_+ &\simeq C(A)(\hat{J}_f/\hat{J}_i)(E_N A_{(20)N} + 3E_P A_{(20)P})^2, \end{aligned} \quad (24)$$

where $C(A) = 0.55A^{-1}$ (mb). Here C is a function of the mass A which roughly represents the effects of distortion and is normalized at the transition to $JT=20$ in ${}^{12}\text{C}$. By using the amplitudes of Table I in these formulas one gets a very good estimate of the calculated cross sections except in cases where the $(KS)=(20)$ amplitudes are at least a factor of 4 smaller than some $(KS)=(21)$ or (01) amplitudes. Of course the formulas are also applicable to weaker transitions where E_N and E_P are unity. The formulas provided a very useful check in the course of our calculations.

Some of the most interesting results of our calculations, such as π^- to π^+ cross-section ratios

which are very large or very small, involve transitions where even the larger of the cross sections is only a few hundredths of a millibarn. This presents difficulty for experiments which is further complicated by the fact that within experimental resolution there are often states known to be of opposite parity to those within the $1p$ space. We have calculated cross sections for some of these states in ${}^{13}\text{C}$. Results will be published later, but we find many transitions with magnitudes between 10^{-2} and 10^{-1} mb and large differences in π^+ and π^- scattering. Therefore, it requires good energy resolution to be sure which state is being excited. The current measurements¹⁹ in ${}^{13}\text{C}$ exhibit many interesting features regarding π^+ to π^- ratios.

There are two earlier published calculations^{21,22} for the (π^+, π^0) cases of Fig. 14 to 16. The authors used different methods and nuclear wave functions than we did, but the results are not markedly different. All the calculations are lower than observation for ${}^{13}\text{C}$ by factors between 2 and 4. In ${}^{10}\text{B}$ all calculations predict that the transition is mainly to the 2^+ state of ${}^{10}\text{C}$ and Ref. 21 obtains the observed magnitude, Ref. 22 gets 60%, and we get 40% of this magnitude. In ${}^7\text{Li}$ we fit the observed magnitude and the other calculations are close but low in some energy regions. There is a difference in the fraction calculated to go to the $\frac{1}{2}$ excited state where we get about 10%, Ref. 22 about 20%, and Ref. 21 about 50%. However, none of the calculations gives a satisfactory account of the observations.

The result of comparing our (π, π') calculations with existing data is quite encouraging. Current experiments will show how well our predictions fare in other cases. In particular, the sensitivity of pions to separate neutron and proton contributions, as in the isospin mixing cases, should provide some very relevant nuclear structure information.

ACKNOWLEDGMENTS

We should like to thank E. Boschitz, H. Thiessen, and B. Zeidman for permission to use their data in our cross-section comparisons. Thanks are also due to R. D. Lawson for comments and careful reading of the manuscript. This work was performed under the auspices of the U. S. Dept. of Energy.

APPENDIX A

The transition density matrix elements of Table I can be used to calculate transitions for any one-body operator. It may be more convenient to use the jj representation. Such amplitudes can be

obtained from the entries in Table I by the transformation

$$\langle J_f T_f \| [b_{j_1 t_3}^\dagger \times \bar{b}_{j_2 t_3}]_g \| J_i T_i \rangle = \sum_{KS} (\hat{j}_1 \hat{j}_2 \hat{K} \hat{S})^{1/2} \begin{pmatrix} 1 & \frac{1}{2} & j_1 \\ 1 & \frac{1}{2} & j_2 \\ K & S & g \end{pmatrix} A_{g(KS)t_3}, \quad (\text{A1})$$

where $\bar{b}_{j m t_3} = (-1)^{j+m} b_{j-m t_3}$ and the bracket is a $9J$ symbol.

¹T.-S. H. Lee and F. Tabakin, Nucl. Phys. A226, 253 (1974).

²S. Cohen and D. Kurath, Nucl. Phys. 73, 1 (1965).

³L. S. Kisslinger, Phys. Rev. 98, 761 (1955); G. E. Edwards and E. Rost, Phys. Rev. Lett. 26, 785 (1971); D. A. Sparrow, Nucl. Phys. A276, 365 (1977), and references therein.

⁴T. J. Londergan, K. W. McVoy, and E. J. Moniz, Ann. Phys. (N.Y.) 86, 147 (1974).

⁵R. A. Eisenstein and F. Tabakin, Comp. Phys. Commun. 12, 237 (1976).

⁶D. M. Brink and G. R. Satchler, *Angular Momentum* (Oxford Univ. Press, London, 1968).

⁷D. H. Gloeckner, Argonne National Lab. Report No. ANL-8113, 1974.

⁸A. R. Poletti, E. K. Warburton, and D. Kurath, Phys. Rev. 155, 1096 (1967).

⁹J. Piffaretti, R. Corfu, J. P. Egger, P. Gretillat, C. Luke, E. Schwarz, C. Perrin, and B. M. Freedom, Phys. Lett. 71B, 324 (1977).

¹⁰D. Kurath, Nucl. Phys. 14, 398 (1960).

¹¹E. T. Boschitz, in *Proceeding of the International Conference on High Energy Physics and Nuclear Structure, Zurich, 1977*, edited by M. P. Locher (Birkhauser, Basel, Switzerland, 1978).

¹²J. Bolger, E. Boschitz, R. Mischke, A. Nagel, W. Saathoff, C. Wiedner, and J. Zichy (unpublished).

¹³D. F. Geesaman, C. Olmer, B. Zeidman, R. L. Boudrie, R. H. Siemssen, J. F. Amann, C. L. Morris, H. A. Thiessen, G. R. Burleson, M. J. Devereux, R. E. Segel, and L. W. Swenson, Phys. Rev. C 18, 2223 (1978).

¹⁴R. J. Peterson *et al.* (private communication).

¹⁵E. G. Adelberger, R. E. Marrs, K. A. Snover, and J. E. Bussolletti, Phys. Rev. C 15, 484 (1977).

¹⁶N. Kumar, Nucl. Phys. A225, 221 (1974).

¹⁷E. K. Warburton, J. W. Olness, S. D. Bloom, and A. R. Poletti, Phys. Rev. 171, 1178 (1968).

¹⁸Y. Shamai, J. Alster, D. Ashery, S. Cochavi, M. A. Moinester, A. Yavin, E. D. Arthus, and D. M. Drake, Phys. Rev. Lett. 36, 82 (1976).

¹⁹D. Dehnhard, S. J. Tripp, M. A. Franey, G. S. Kyle, C. L. Morris, R. L. Boudrie, J. Piffaretti, and H. A. Thiessen, Phys. Rev. Lett. 43, 1091 (1979).

²⁰C. Olmer, D. F. Geesaman, B. Zeidman, S. Chakravarti, T.-S. H. Lee, R. L. Boudrie, R. H. Siemssen, J. F. Amann, C. L. Morris, H. H. Thiessen, G. R. Burleson, M. J. Devereux, R. E. Segel, and L. W. Swenson, Phys. Rev. C 21, 254 (1980), this issue.

²¹W. R. Gibbs, B. F. Gibson, A. T. Hess, G. J. Stephenson, Jr., and W. B. Kaufman, Phys. Rev. Lett. 36, 85 (1976).

²²J. Waszawski and N. Auerbach, Nucl. Phys. A276, 402 (1977).